Journal of
Sensor and Actuator Networks

MDPI

Article

Sensor-Based Detection of Characteristics of Rubber Springs

Leopold Hrabovský *, Jan Blata, Ladislav Kovář, Michal Kolesár and Jaromír Štěpáník

Department of Machine and Industrial Design, Faculty of Mechanical Engineering, VSB—Technical University of Ostrava, 17. Listopadu 2172/15, 708 00 Ostrava-Poruba, Czech Republic; jan.blata@vsb.cz (J.B.); ladislav.kovar@vsb.cz (L.K.); michal.kolesar@vsb.cz (M.K.); jaromir.stepanik.st@vsb.cz (J.Š.)
* Correspondence: leopold.hrabovsky@vsb.cz

Abstract: Knowledge of experimentally obtained values of elastic deformations of rubber springs induced by applied compressive forces of known magnitudes is essential for the selection of rubber springs with optimal properties, which are used to dampen vibrations transmitted to the supporting parts of vibrating machines. This paper deals with the laboratory measurement of the characteristics of rubber springs using two types of sensors which sense the instantaneous value of the compressive force acting on the compressed spring. When using a strain tensometric force sensor, the magnitude of the measured pressure forces was evaluated by the DeweSoft DS-NET system, which was connected to an ethernet LAN, so the measured data could be processed, analysed and stored by any computer on the network. The characteristics of eight types of rubber springs were measured in two ways on laboratory equipment, and the spring stiffnesses were calculated from the measured data. Experiments have shown that the actual stiffnesses of rubber springs are lower compared to the values stated by the manufacturer, in the least favourable case, by 33.6%. It has been shown by measurements that at the beginning of the loading of the rubber spring, its compression is gradual, and the stiffness increases slowly, which is defined as the progressivity of the spring.

Keywords: force sensor; rubber spring; elastic deformation; spring characteristics and stiffness

Academic Editor: Lei Shu

Received: 16 November 2024
Revised: 7 January 2025
Accepted: 7 January 2025
Published: 9 January 2025

Citation: Hrabovský, L.; Blata, J.; Kovář, L.; Kolesár, M.; Štěpáník, J. Sensor-Based Detection of Characteristics of Rubber Springs. *J. Sens. Actuator Netw.* **2025**, *14*, 5. https://doi.org/10.3390/jsan14010005

1. Introduction

Spring stiffness [1], also known as spring constant or spring moment, is a measure of how much force is required to compress a compression spring for a certain distance. Spring stiffness [2] is a physical quantity that indicates the rate of change in length relative to the magnitude of the external force acting during elastic deformation.

The purpose of this study is to obtain, by sensor measurements, a mathematical relationship between the compressive forces acting on rubber springs (which are digital inputs) and their elastic deformation. The characteristics of rubber springs obtained by laboratory measurements [3] are a valuable asset in the selection of real springs that are installed in vibrating machines. The benefit can be justified by the fact that the spring stiffness values stated in manufacturers' catalogues are often different from the stiffness values of the actual springs.

Steel or rubber springs are widely used in industrial operations to dampen vibrations transmitted to the substructure of vibration machines. The paper [4] presents the theoretical calculations of the pallet brake, which is a crucial element of the pallet locking system (using cylindrical compression springs) of the conceptual variant of the automatic parking system.

Soliman et al. in their paper [5] investigated the effect of suspension spring stiffness on vehicle dynamics. They used a chassis dynamometer to perform experimental work. The predicted results were compared with experimental measurements.

The structure of a mechanical spring with adjustable stiffness was presented in the article [6] and outlined the solution of temperature control systems. The spring was tested in an experimental setup and compiled test results were provided. Selected results were shown in the article for different excitations and operating temperatures. The obtained results show that the spring built using SMA has many interesting properties.

The paper [7] examined the spatial variation of the Winkler spring stiffness constants.

Due to the need to choose the optimal stiffness of springs that support the oscillating masses of vibrating machines, it is often necessary in practice to verify whether the stiffness of the springs corresponds to the stiffness stated in the spring manufacturers' catalogues. The actual spring stiffness determined by measuring the compressive/tensile force depending on compression/extension is often different from the catalogue value of the spring stiffness [8,9]. For the purpose of determining the spring characteristics, the laboratory equipment described in this article was designed at the Department of Machine and Industrial Design, Faculty of Mechanical Engineering, VSB-Technical University of Ostrava.

Smooth-running conveying equipment—namely, vibratory conveyors with microshafts or vibrating sorters with mechanical exciter, electromagnetic vibrators or vibration exciters consisting of a pair of vibration electric motors [10]—use the harmonic vibration of the trough or sorting screens [11,12] to move grains of bulk material.

In Ref. [13], L.L. Howell et al. investigated the spring stiffness equivalent to a pseudo-rigid body, and new modelling equations were proposed therein. The result is a simplified method of modelling the force/deflection relationships of large-deflection members in compliant mechanisms.

The articles [14,15] represented a structural design as well as a created 3D model used for subsequent physical implementation of a validation device that allows for measuring the force as well as the shortening of a coiled pressure spring during laboratory experiments.

In the article [16], the authors R. Lefanti et al. conducted an evaluation of the reliability of the elastomeric silent block based on the shape factor, and the materials used were developed.

The authors concluded that silent block failure is caused by radial loads and axial displacement leading to fatigue and wear. They created a test rig to evaluate reliability.

In the article [17], J. Ziobro presented a mechanical calculation of the silent block model. Based on the model, he performed a 3D numerical analysis using two types of rubber bushings with different hardness. When using all-rubber bushings for silent blocks, the author recommends optimal damping properties achieved by using a lower hardness of these elements. A satisfactory compromise between stability and damping characteristics can also be achieved by using specially shaped bushings that are made of harder rubber.

The following studies [18,19], for example, deal with the analysis of the characteristic properties of silent blocks used in automobiles. The article [18] deals with an aluminium silent block that connects the front suspension mounting and the road wheels subjected to high technical stress. Over time, the connecting part of these products breaks due to insufficient strength.

Fedotov et al. in the article [19] stated the test equipment and test results that were carried out in the research laboratory of the VSGUTU Car Department. The main purpose of the laboratory tests was to obtain experimental data for the development of mathematical models of the functioning of car suspension silent blocks for the development of a diagnostic method. The authors have shown in this article that the compression resistance of a silent

block increases linearly with increasing load. Silent blocks change their compression resistance first slowly with increasing load and then more steeply.

In the study [20], Hatekar et al. analysed using static and dynamic load cases using virtual simulation (MSC.ADAMS) the stiffness of the casing. Based on the stiffness and load cycle calculation, the profile of the elastomer was finalized, and the material property was chosen to meet all the required parameters of performance and service life.

The operational reliability of vibrating machines [21–23] is largely determined by the reliability of suspension elements that use silent blocks. In this regard, currently one of the urgent tasks of technical diagnostics is to determine the technical condition of the suspension in operation. Any suspension of a vibrating conveyor (sorter) contains many details, which complicates its diagnosis and requires highly qualified personnel and special equipment. The detection of suspension faults is often not carried out by diagnostics, but by the structural parameters of the technical condition, determined during the disassembly and defecation of its parts. Failure of any suspension component can reduce operational reliability and directly affect the active safety of the vibrating machine or operator.

The main content of the paper [24] by the authors Misol, Algermissen and Monner, was the evaluation of the excitation of the windshield, which was realized by an electrodynamic exciter (shaker). The authors of the windshield measurements assumed that the glass was embedded in the rubber, which acted as a spring dampening the vibrations when the vehicle moved.

Rubber springs are widely used in industry as anti-vibration components providing many years of service, as shown in Ref. [25]. Luo and Wu in the article [25] state that the purpose of the FE analysis is to obtain improved fatigue life of the spring. It is shown in the paper that a quasi-static simulation for rubber springs using nonlinear software can provide good indication for product design and failure analysis.

M. Berg in Ref. [26] proposed a nonlinear dynamic model of a rubber spring and focused on the representation of the mechanical behaviour of rubber suspension components in rail vehicle dynamics.

For the analysis of railway vehicle dynamics, the article [27] by R. Luo et al. designed a simple and more accurate nonlinear rubber spring model. The characteristics of dynamic stiffness and damping were investigated through both simulations and lab tests with various displacement amplitude and frequency.

In the article [28] by Wu and Shangguan, a model characterizing the relations between excitation frequencies as well as excitation amplitudes and the dynamic performances of a rubber isolator was presented. Measurements showed that dynamic characteristics of the rubber isolators relate to excitation amplitudes and excitation frequencies.

In the article [29], H. Shi and P. Wu created a nonlinear dynamic model for a rubber spring and subsequently used it to describe the mechanical behaviour of rubber mounts in the suspension system of a railroad vehicle. In this paper, the dynamic stiffness and damping characteristics in relation to the applied displacement amplitude and frequency were investigated by means of simulations and measurements.

In Ref. [30], Misaji et al. described a method for analysing nonlinear vibration response. They verified the appropriateness and accuracy of this method by directly comparing the analytical results with the experimental results for the dynamic response of a system.

Austin et al. in Ref. [31] reported that soft springs provide higher torque resolution at the cost of system bandwidth, whereas stiff springs provide a fast response but lower torque resolution. Nonlinear springs potentially incorporate the benefits of both soft and stiff springs, but such springs are often large. A nonlinear spring design was recently proposed that combines a variable radius camera with a rubber elastic element, enabling a compact spring design.

Based on the above-mentioned research of technical articles dealing with measuring spring stiffness and the conclusions therein, it is necessary to use optimal types of silent blocks in vibrating machines. Given this conclusion, the laboratory equipment presented in this article was designed.

The main objective of this study was to use sensors to detect the magnitude of the compressive force acting on the rubber spring, thus enabling monitoring, data collection and storage for the purpose of the autonomous operation of vibration machines. The ability to detect the actual instantaneous magnitudes of the applied forces by sensors in real time and to use these digital values to communicate with the control unit allows for increasing the safety and reliability of the operation of the vibration machine [31,32] and its key machine parts, which can also include springs. A significant aspect is the reduction of the risk of accidents both during maintenance and working activities and the assurance of functionality without the need for human presence due to the use of automation and sensor monitoring.

The novelty and innovation can be traced in the designed laboratory device. The laboratory device allows two (independent) methods to determine the exact value of the stiffness of a rubber spring by measurement. The measurement can obtain the value of the compression of the rubber spring and also the value of the pressure force that deforms the rubber spring.

2. Materials and Methods

In the technical literature, instructions are presented on how to select a suitable spring for a given type of vibrating machine; however, often there is a lack of instructions and a methodological procedure on how to correctly and accurately determine the stiffness of a silent block. In this article, we have tried to present one of the options for determining the stiffness of rubber. Stiffness is determined from the values detected by sensors. The signals are processed by the DeweSoft DS-NET measuring system (DEWETRON Inc., East Greenwich, RI, USA) and sent to a PC via a Wi-Fi router, which evaluates them.

Vibrating conveyors/sorters use the inertial forces on the individual grains of the conveyed material to move/sort the material. The inertial forces are generated by the harmonic oscillating motion of the trough (micro-rotor conveyors)—see Figure 1—in which the material particles are separated from the trough surface at a certain phase of the transport time (the vertical component of the acceleration of the oscillating motion is greater than the acceleration due to gravity).

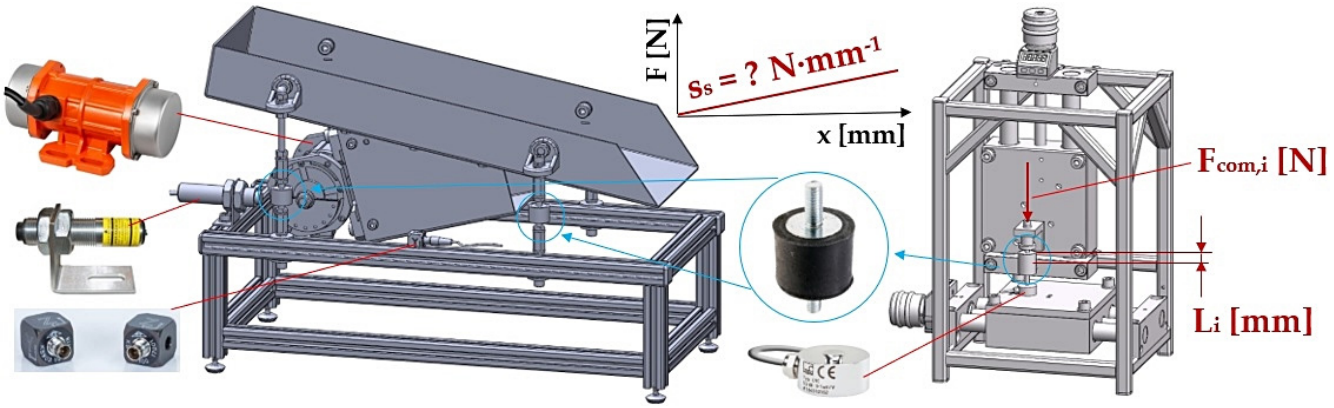

Figure 1. Model of vibrating conveyor with asynchronous single-phase vibrating electric motor.

The source of the harmonic oscillations is the exciter, which is usually firmly connected to the trough. The trough is supported/suspended by steel or rubber (silent block) springs. The springs allow the trough to perform harmonic motion and at the same time prevent the

transmission of dynamic forces to the substructure; for this reason there is an attempt to select springs with the lowest possible stiffness s_s [$N \cdot m^{-1}$]. The stiffness of the springs also determines whether the vibration machine will operate in the sub-resonant ($z < 1$), resonant ($z = 0.85 \div 0.95$) or supra-resonant ($z > 1 \div 5$) zone, where $z = \omega/\omega_0$, $\omega = 2 \cdot \pi \cdot f$ [s^{-1}] is the operating frequency of the machine, f [Hz] is the frequency of vibration generated by the exciter, and ω_0 [s^{-1}] is the natural frequency of the machine (1). The stiffness of the springs supporting the trough of mass m [kg] (including the mass of the conveyed material placed on the trough) can be determined according to (1).

$$s_s = \omega_0 \cdot m \left[N \cdot m^{-1} \right], \quad (1)$$

In many springs that are in use, especially in the case of the frequently used helical springs or rubber springs, the dependence of the deformation (compression) x [m] due to the applied force F [N] is almost linear [20], and in graphical expression it is a line. The slope of this line gives the spring stiffness s_s [$N \cdot m^{-1}$], which is a constant expressing the force required to deform the spring per unit [4]. In the case of a direct proportionality between force and deflection, such behaviour can be expressed mathematically as follows by Hooke's law (2):

$$F = s_s \cdot x [N], \quad (2)$$

where F [N] is the spring force, and x [m] is the spring deflection from the resting state.

A body suspended by a spring, or supported by a spring, is one of the simplest mechanical oscillators, i.e., a system that performs oscillations. If damping is neglected, a body of mass m [kg] on a spring of stiffness s_s [$N \cdot m^{-1}$] performs harmonic oscillations of natural angular frequency ω_0 [$rad \cdot s^{-1}$] (1).

The spring characteristic is generally a curve expressing the dependence between the force acting on the spring and its elastic deformation. The area under the curve corresponds to the delivered work W [J] (3) required for a certain deformation of the spring or the accumulated potential energy E_p [J] of the loaded spring.

$$E_p = W = 0.5 \cdot F \cdot x = 0.5 \cdot s_s \cdot x^2 [J], \quad (3)$$

In order to verify the catalogue values [33,34] of the stiffness of rubber springs, a laboratory device was designed and constructed which allows for the measurement of the elastic deformation of rubber springs, which are called "silent blocks", depending on the magnitude of the applied compressive force, using sensors [35,36] and positioning units with a digital indicator [37]. This was carried out in a laboratory at the Department of Machine and Industrial Design, Faculty of Mechanical Engineering, VSB-Technical University of Ostrava.

Figure 2 presents the first variation of the measurement of compression rubber spring characteristics. The bolt of the tested silent block 3 was attached to the sled of the positioning unit (long positioning table PT7312-PA [37]) 4. The measurements were carried out on a total of eight types of silent blocks, made of NR/SBR rubber with a hardness of 55° shA, with the bolt having an M6 thread. Four silent blocks were of diameter D = 20 mm and lengths H_0 = 10, 15, 20 and 25 mm, while the remaining four silent blocks were of diameter D = 25 mm and lengths H_0 = 15, 20, 25 and 30 mm. The positioning unit 4 was attached to the steel frame 1 of the laboratory apparatus similarly to digital force gauge DST-220A [35], with a measuring range of $0 \div 1000$ N.

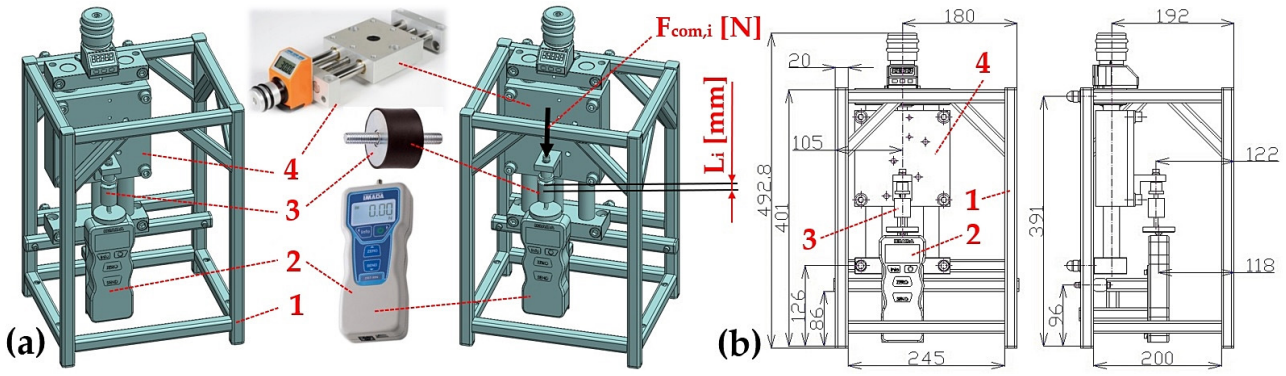

Figure 2. Laboratory device detecting rubber spring characteristics—variation 1, (**a**) 3D model created in SolidWorks™ Premium 2012 × 64 SP5.0 software (SOLIDWORKS Corporation.; Vélizy; France), (**b**) 2D sketch created in AutoCAD 2024 software (Autodesk, Inc., Mill Valley, CA, USA). 1—steel frame, 2—digital force gauge, 3—silent block, 4—positioning unit.

By manually rotating the locking bolt of the positioning unit 4 in the appropriate direction, the shank of the rubber spring bolt 3 was brought closer/farther away from the measuring surface of the digital force gauge 2. At the moment when the shank of the bolt of the rubber spring 3 reached the measuring surface of the digital force gauge 2, the digital indicator of the positioning unit 4 and the digital force gauge 2 were reset. By turning the locking bolt of the positioning unit 4, the sled was moved vertically by the desired amount L_i [m]. The value of the applied compressive force $F_{com,i}$ [N] was read on the digital force gauge 2 for the compression value L_i [m] (i.e., the length of the rubber spring $H_i = H_0 - L_i$ [m]) of the rubber spring 3.

The procedure was repeated until the predetermined maximum compression $_{Li} = L_i = L_{max}$ [m] of the rubber spring 3 was reached. By turning the locking bolt of the positioning unit 4 in the reverse direction, the values of the compressive force $F_{rel,i}$ [N] at the compression value L_i [m] of the rubber spring 3 were measured on the digital force gauge 2. The values of the measured compressive forces by the digital force gauge 2 can be recorded using the Force Logger software [38] and saved on a computer.

Figure 3 presents the second variation of measuring the characteristics of a compression rubber spring. Tension pressure sensor C9B-1kN 2 [36] with a measuring range of 0 N to 1000 N was mechanically attached to the sled of the horizontally positioned positioning unit 4.

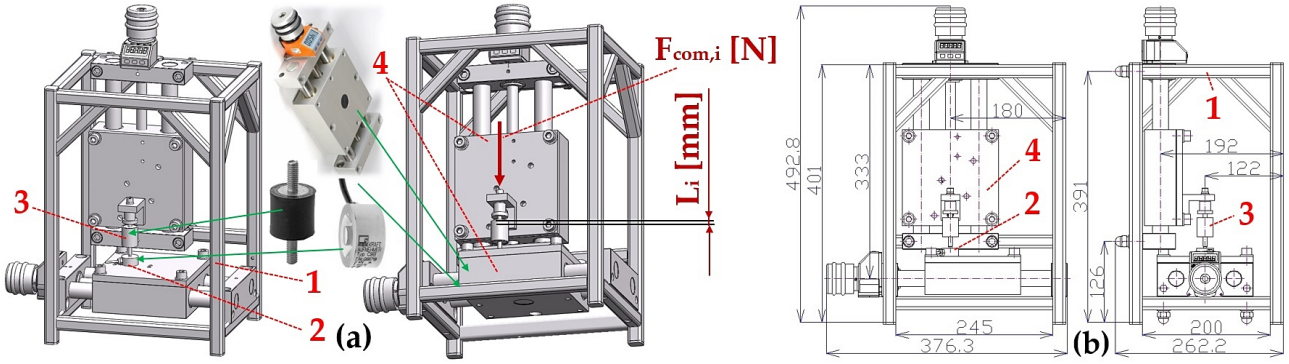

Figure 3. Laboratory device detecting rubber spring characteristics—variation 2, created in SolidWorks™ Premium 2012 × 64 SP5.0 software, (**a**) 3D model, (**b**) 2D sketch. 1—steel frame, 2—digital force gauge, 3—silent block, 4—positioning unit.

By manually rotating the locking bolt of the vertically positioned positioning unit 4 in the appropriate direction, the shank of the rubber spring screw 3 was brought closer/farther

away from the measuring surface of the tension pressure sensor 2. Using the DEWESoft X2 SP5 software [39], the signals of the measured quantity (pressure forces $F_{com,i}$ [N]) were recorded, having been detected by the DEWESoft DS-NET measuring apparatus [40]; see Figure 4.

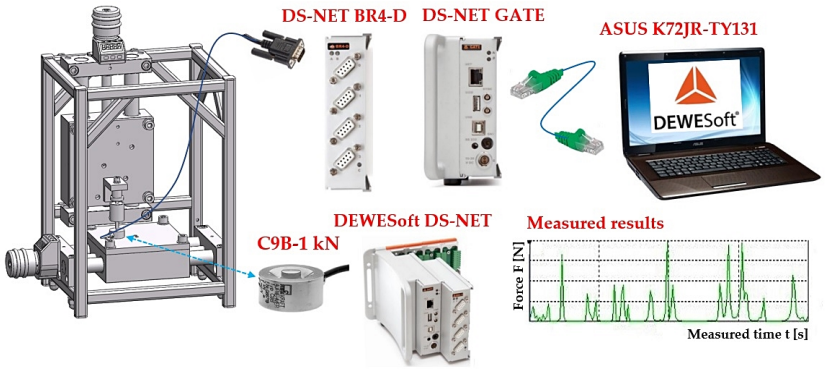

Figure 4. Measurement chain—a sequence of interconnected instruments and devices enabling the detection and processing of measured signals.

The cable of the tension pressure sensor C9B-1 kN—see Figure 4—fitted with a D-Sub 9-pin plug, was connected to the DS NET BR4 module [40]. The RJ45 connectors of the network cable connect the DS GATE module [40] to a PC (ASUS K72JR-TY131) running the DEWESoft X2 SP5 software [39].

The constructed laboratory device that allows detection of the magnitude of compressive forces acting on rubber springs is presented in Figure 5.

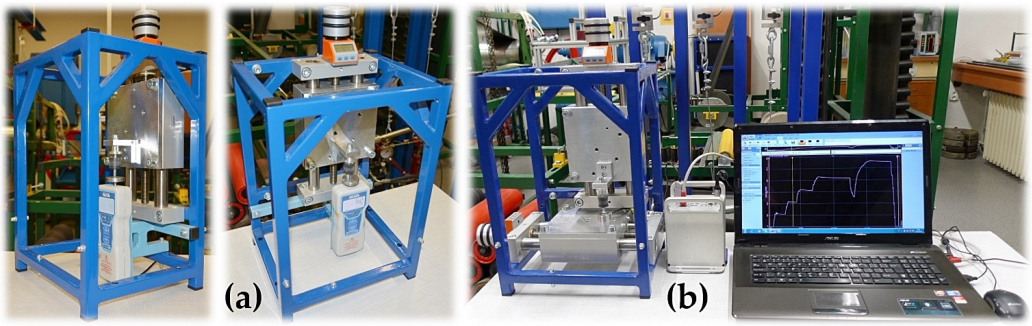

Figure 5. Measurement of the rubber spring compressive force with (**a**) digital force gauge DST-220A, and (**b**) tension pressure sensor C9B-1 kN.

3. Results

Compressive forces of compressed rubber springs ϕ20 mm, with lengths in an unloaded state of H_0 = 10, 15, 20 and 25 mm and ϕ25 mm, H_0 = 15, 20, 25 and 30 mm were measured on the laboratory equipment; see Figure 5. All types of rubber springs were made of NR/SBR rubber with a hardness of 55° shA.

The values of n times repeated measurements of compressive forces under the same technical conditions were, for individual compression of rubber springs, displayed in the software Force Logger [38] using the digital force gauge DST-220A, or in the software DEWESoft X2 SP5 using the tension pressure sensor C9B and recorded in tables; see Sections 3.1 and 3.2.

3.1. Detection of Forces Acting on Silent Blocks with a Digital Force Gauge

Table 1 shows the measured values of the compressive force $F_{com,i}$ [N] of a silent block ϕ20 mm with a length in the unloaded state of H_0 = 10 mm during its compression,

i.e., deformation L_i [m]. Additionally presented in Table 1 are the measured values of the compressive force $Frel_{,i}$ [N] when the silent block is released from the length $H_i = H_0 - L_i$ [m]. The maximum possible compression of the silent block is $L_i = L_{max}$ [m], from which the minimum silent block length $H_N = H_0 - L_{.max}$ [m] can be expressed.

Table 1. Rubber spring D = 20 mm; length when not loaded H_0 = 10 mm.

i	1		2		3		4		5						
L_i	$F_{com,1}$	$F_{rel,1}$	$F_{com,2}$	$F_{rel,2}$	$F_{com,3}$	$F_{rel,3}$	$F_{com,4}$	$F_{rel,4}$	$F_{com,5}$	$F_{rel,5}$	F_{com} [1]	$\kappa_{5\%,5}$	F_{rel} [1]	$\kappa_{5\%,5}$	$s_{scom,i}$
mm	N														$N \cdot mm^{-1}$
0	0	0	0	0	0	0	0	0	0	0	0	0	0	0	-
0.2	31	23	34	24	34	27	32	25	32	27	32.6	2.0	25.2	2.5	181.1
0.6	119	96	126	99	124	99	121	100	124	98	122.8	3.9	98.4	2.0	204.7
0.9	201	158	193	162	194	167	191	161	193	162	194.4	4.6	162.0	3.5	216.0
1.3	287	252	286	256	287	257	283	258	285	256	285.6	2.2	255.8	2.6	219.7
1.7	369	369	371	371	373	373	371	371	372	372	371.2	1.8	371.2	1.8	218.4

[1] see Figure 6.

Figure 6 presents the dependence of the compressive force acting on a rubber spring ϕ20 mm with length in the unloaded state of $H_0 = 10 \div 25$ mm and its elastic deformation.

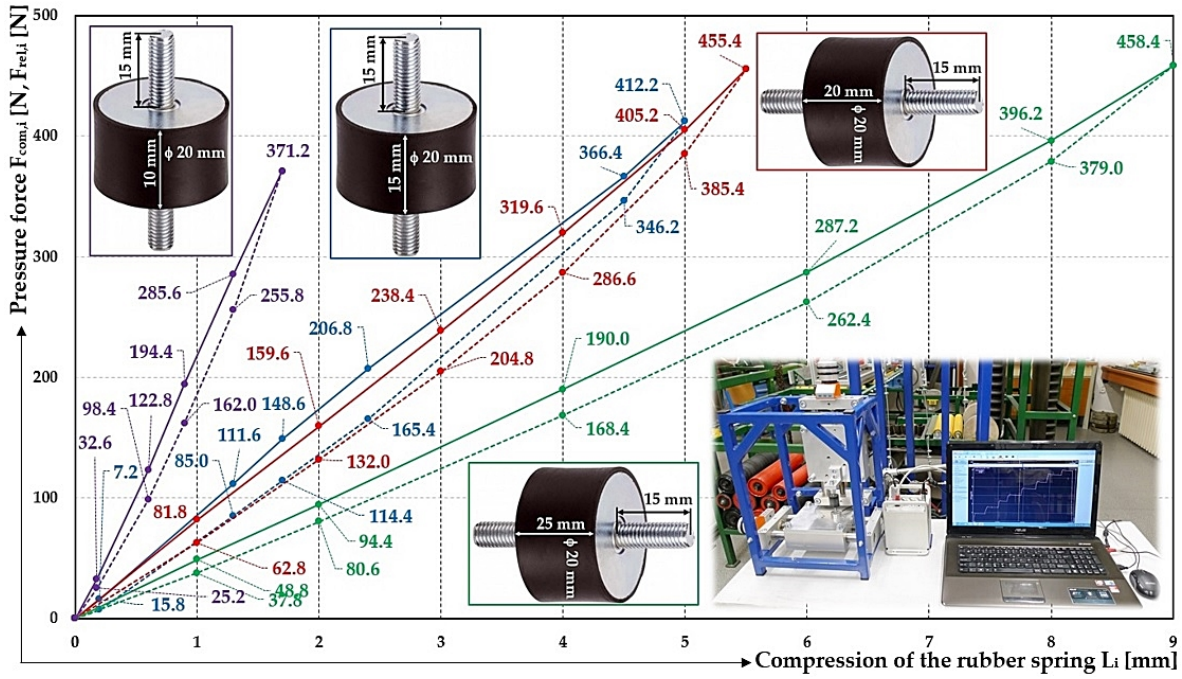

Figure 6. Graph of the dependence of the compressive force acting on a rubber spring ϕ20 mm with length in the unloaded state of $H_0 = 10 \div 25$ mm and its elastic deformation. H_0 (●) 10 mm, (●) 15 mm, (●) 20 mm, (●) 25 mm.

The resulting calculated compression force F_{com} [N] or release force F_{rel} [N] of the form (4), using Student's distribution [41], is given in Table 1

$$F_{com}(F_{rel}) = F_{com}(F_{rel}) \pm \kappa_{\alpha,n} = F_{com}(F_{rel}) \pm \kappa_{5\%,5}[N],\ \kappa_{5\%,5} = t_{\alpha,n} \cdot s = t_{5\%,5} \cdot s \quad (4)$$

where $F_{com}(F_{rel})$ [N] is the arithmetic mean of all (n = 5—number of repeated measurements) measured values of $F_{com,i}(F_{rel,i})$ [N], $\kappa_{\alpha,n}$ [-] is the marginal error, $t_{\alpha,n}$ [-] ($t_{5\%,5}$ = 2.78) is the Student's coefficient for the risk α [%] (α = 5%) and the confounding coefficient P [%] (P = 95%) [41], and s [-] is the sample standard deviation of the arithmetic mean.

Table 2 shows the measured values of the compressive force $F_{com,i}$ [N] and $F_{rel,i}$ [N] when compressing and releasing a silent block ϕ20 mm with length in the unloaded state

of H_0 = 15 mm. In Ref. [34], the maximum compression L_{max} = 3.75 mm, the maximum load F_{max} = 352 N and the stiffness of the silent block s_s = 94 N·mm^{-1} are given for this type of silent block.

Table 2. Rubber spring D = 20 mm; length when not loaded H_0 = 15 mm.

i	**1**		**2**		**3**		**4**		**5**						
L_i	$F_{com,1}$	$F_{rel,1}$	$F_{com,2}$	$F_{rel,2}$	$F_{com,3}$	$F_{rel,3}$	$F_{com,4}$	$F_{rel,4}$	$F_{com,5}$	$F_{rel,5}$	F_{com} [1]	$\kappa_{5\%,5}$	F_{rel} [1]	$\kappa_{5\%,5}$	$s_{scom,1}$
mm							**N**								**N·mm^{-1}**
0	0	0	0	0	0	0	0	0	0	0	0	0	0	0	-
0.2	16	7	16	7	17	7	14	8	16	7	15.8	1.3	7.2	0.6	79.0
1.3	116	83	111	87	107	85	115	86	109	84	116.6	5.4	85.0	2.1	85.8
2.0	155	110	150	115	148	72	144	117	146	115	148.6	5.4	114.4	3.1	87.4
2.8	213	161	208	166	148	115	203	168	205	165	206.8	5.1	165.4	3.3	86.2
4.5	366	342	365	346	368	346	369	349	364	348	366.4	2.9	346.2	3.2	81.4
5.0	405	405	415	415	414	414	413	413	414	414	412.2	5.0	412.2	5.0	82.4

[1] see Figure 6.

Table 3 shows the measured values of the compressive force $F_{com,i}$ [N] and $F_{rel,i}$ [N] when compressing and releasing a silent block ϕ20 mm with length in the unloaded state of H_0 = 20 mm. In Ref. [34], the maximum compression L_{max} = 5 mm, the maximum load F_{max} = 260 N and the stiffness of the silent block s_s = 52 N·mm^{-1} are given for this type of silent block.

Table 3. Rubber spring D = 20 mm; length when not loaded H_0 = 20 mm.

i	**1**		**2**		**3**		**4**		**5**						
L_i	$F_{com,1}$	$F_{rel,1}$	$F_{com,2}$	$F_{rel,2}$	$F_{com,3}$	$F_{rel,3}$	$F_{com,4}$	$F_{rel,4}$	$F_{com,5}$	$F_{rel,5}$	F_{com} [1]	$\kappa_{5\%,5}$	F_{rel} [1]	$\kappa_{5\%,5}$	$s_{scom,i}$
mm							**N**								**N·mm^{-1}**
0	0	0	0	0	0	0	0	0	0	0	0	0	0	0	-
1.0	81	62	84	64	81	62	82	62	81	64	81.8	1.7	62.8	1.7	81.8
2.0	159	128	163	134	159	133	159	131	158	134	159.6	2.4	132.0	3.5	79.8
3.0	239	198	242	207	238	205	237	206	236	208	238.4	2.9	204.8	4.7	79.5
4.0	319	282	323	288	319	287	318	286	319	290	319.6	2.4	286.6	3.6	79.9
5.0	397	381	411	389	405	385	406	384	407	388	405.2	5.8	385.4	4.3	81.0
5.5	452	452	458	458	455	455	454	454	458	458	455.4	3.6	455.4	3.6	82.8

[1] see Figure 6.

Table 4 shows the measured values of the compressive force $F_{com,i}$ [N] and $F_{rel,i}$ [N] when compressing and releasing a silent block ϕ20 mm with length in the unloaded state of H_0 = 25 mm. In Ref. [34], the maximum compression L_{max} = 6.25 mm, the maximum load F_{max} = 310 N and the stiffness of the silent block s_s = 50 N·mm^{-1} are given for this type of silent block.

Table 4. Rubber spring D = 20 mm; length when not loaded H_0 = 25 mm.

i	**1**		**2**		**3**		**4**		**5**						
L_i	$F_{com,1}$	$F_{rel,1}$	$F_{com,2}$	$F_{rel,2}$	$F_{com,3}$	$F_{rel,3}$	$F_{com,4}$	$F_{rel,4}$	$F_{com,5}$	$F_{rel,5}$	F_{com} [1]	$\kappa_{5\%,5}$	F_{rel} [1]	$\kappa_{5\%,5}$	$s_{scom,i}$
mm							**N**								**N·mm^{-1}**
0	0	0	0	0	0	0	0	0	0	0	0	0	0	0	-
1.0	50	36	48	38	49	38	48	38	49	39	48.8	1.1	37.8	1.3	48.8
2.0	95	78	95	81	95	82	93	80	94	82	94.4	1.3	80.6	2.2	47.2
4.0	194	163	190	168	190	171	187	169	189	171	190.0	2.8	168.4	4.0	47.5
6.0	292	258	288	264	286	264	283	262	287	264	287.2	3.9	262.4	3.3	47.9
8.0	402	375	399	380	397	382	392	378	391	380	396.2	6.5	379.0	3.5	49.5
9.0	456	456	459	459	462	462	456	456	459	459	458.4	3.3	458.4	3.3	50.9

[1] see Figure 6.

The resulting calculated compression force $F_{com,i}$ [N] or release force $F_{rel,i}$ [N] of the form (4), using Student's distribution [41], is given in Table 4.

Table 5 shows the measured values of the compressive force $F_{com,i}$ [N] of a silent block ϕ25 mm with a length in the unloaded state of H_0 = 15 mm during its compression, i.e., deformation L_i [m]. Also presented in Table 5 are the measured values of the compressive force $F_{rel,i}$ [N] when the silent block is released from the length $H_i = H_0 - L_i$ [m]. In Ref. [34], the maximum compression L_{max} = 3.75 mm, the maximum load F_{max} = 687 N and the stiffness of the silent block s_s = 183 N·mm^{-1} are given for this type of silent block.

Table 5. Rubber spring D = 25 mm; length when not loaded H_0 = 15 mm.

i	**1**		**2**		**3**		**4**		**5**						
L_i	$F_{com,1}$	$F_{rel,1}$	$F_{com,2}$	$F_{rel,2}$	$F_{com,3}$	$F_{rel,3}$	$F_{com,4}$	$F_{rel,4}$	$F_{com,5}$	$F_{rel,5}$	F_{com} [1]	$\kappa_{5\%,5}$	F_{rel} [1]	$\kappa_{5\%,5}$	$s_{scom,i}$
mm							**N**								**N·mm^{-1}**
0	0	0	0	0	0	0	0	0	0	0	0	0	0	0	-
0.4	54	42	53	43	52	42	51	42	53	42	52.6	1.5	42.2	0.6	131.5
0.8	106	89	105	91	104	91	103	90	104	90	104.4	1.5	90.2	1.1	130.5
1.2	159	139	161	139	160	138	157	141	158	140	159.0	0.1	139.4	1.5	132.5
1.6	215	192	217	194	215	193	213	191	214	193	214.8	1.8	192.6	1.5	134.3
2.0	272	252	275	251	272	251	272	253	274	252	273.0	2.1	251.8	1.1	136.5
2.4	331	310	335	312	332	313	331	314	333	313	332.4	2.2	312.4	2.0	138.5
2.8	396	379	397	378	396	382	394	382	395	382	395.6	1.5	380.6	2.9	141.3
3.2	454	454	453	453	457	457	456	456	457	457	455.4	2.6	455.4	2.6	142.3

[1] see Figure 7.

Table 6 shows the measured values of the compressive force $F_{com,i}$ [N] and $F_{rel,i}$ [N] when compressing and releasing a silent block ϕ25 mm with length in the unloaded state of H_0 = 20 mm. In Ref. [34], the maximum compression L_{max} = 5 mm, the maximum load F_{max} = 602 N and the stiffness of the silent block s_s = 120 N·mm^{-1} are given for this type of silent block.

Table 6. Rubber spring D = 25 mm; length when not loaded H_0 = 20 mm.

i	**1**		**2**		**3**		**4**		**5**						
L_i	$F_{com,1}$	$F_{rel,1}$	$F_{com,2}$	$F_{rel,2}$	$F_{com,3}$	$F_{rel,3}$	$F_{com,4}$	$F_{rel,4}$	$F_{com,5}$	$F_{rel,5}$	F_{com} [1]	$\kappa_{5\%,5}$	F_{rel} [1]	$\kappa_{5\%,5}$	$s_{scom,i}$
mm							**N**								**N·mm^{-1}**
0	0	0	0	0	0	0	0	0	0	0	0	0	0	0	-
1.0	93	71	95	65	94	71	91	69	94	70	93.4	2.0	69.2	3.1	93.4
2.0	176	140	178	139	179	141	174	141	179	140	177.2	3.1	140.2	1.1	88.6
3.0	251	213	256	214	254	214	249	213	252	213	252.4	3.6	213.4	3.6	84.1
4.0	337	303	341	304	339	303	333	304	336	303	337.2	3.9	303.4	0.8	84.3
5.0	446	446	447	447	446	446	444	444	445	445	445.6	1.5	445.6	1.5	89.1

[1] see Figure 7.

Table 7 shows the measured values of the compressive force $F_{com,i}$ [N] and $F_{rel,i}$ [N] when compressing and releasing a silent block ϕ25 mm with length in the unloaded state of H_0 = 25 mm. In Ref. [34], the maximum compression L_{max} = 6.25 mm, the maximum load F_{max} = 675 N and the stiffness of the silent block s_s = 108 N·mm^{-1} are given for this type of silent block.

Table 7. Rubber spring D = 25 mm; length when not loaded H_0 = 25 mm.

i	**1**		**2**		**3**		**4**		**5**						
L_i	$F_{com,1}$	$F_{rel,1}$	$F_{com,2}$	$F_{rel,2}$	$F_{com,3}$	$F_{rel,3}$	$F_{com,4}$	$F_{rel,4}$	$F_{com,5}$	$F_{rel,5}$	F_{com} [1]	$\kappa_{5\%,5}$	F_{rel} [1]	$\kappa_{5\%,5}$	$s_{scom,i}$
mm							**N**								**N·mm^{-1}**
0	0	0	0	0	0	0	0	0	0	0	0	0	0	0	-
1.0	77	60	74	58	76	61	76	61	75	60	75.6	1.5	60.0	1.4	75.6
2.0	146	123	144	122	144	125	145	122	144	124	144.6	1.3	123.2	1.8	72.3
3.0	214	189	212	191	211	192	212	192	211	191	212.0	1.4	191.0	1.4	70.7
4.0	279	256	281	259	280	261	281	262	281	262	280.4	1.3	260.0	3.5	70.1
5.0	347	331	352	335	351	334	353	334	351	332	350.8	2.6	333.2	2.4	70.2
6.0	424	424	426	426	428	428	429	429	427	427	426.8	2.5	426.8	2.5	71.1

[1] see Figure 7.

Table 8 shows the measured values of the compressive force $F_{com,i}$ [N] and $F_{rel,i}$ [N] when compressing and releasing a silent block ϕ25 mm with length in the unloaded state of H_0 = 30 mm. In Ref. [34], the maximum compression L_{max} = 7.5 mm, the maximum load F_{max} = 562 N and the stiffness of the silent block s_s = 75 N·mm^{-1} are given for this type of silent block.

Table 8. Rubber spring D = 25 mm; length when not loaded H_0 = 30 mm.

i	**1**		**2**		**3**		**4**		**5**						
L_i	$F_{com,1}$	$F_{rel,1}$	$F_{com,2}$	$F_{rel,2}$	$F_{com,3}$	$F_{rel,3}$	$F_{com,4}$	$F_{rel,4}$	$F_{com,5}$	$F_{rel,5}$	F_{com} [1]	$\kappa_{5\%,5}$	F_{rel} [1]	$\kappa_{5\%,5}$	$s_{scom,i}$
mm	**N**														**N·mm^{-1}**
0	0	0	0	0	0	0	0	0	0	0	0	0	0	0	-
1.0	66	33	62	36	64	37	61	36	64	33	63.4	2.6	35.0	2.8	63.4
2.0	118	89	122	86	117	84	116	86	113	85	117.2	3.9	86.0	2.1	58.6
3.0	169	139	176	142	168	139	174	143	172	143	171.6	5.0	141.2	3.1	57.3
4.0	223	191	227	191	219	193	229	196	218	194	223.2	6.7	193.0	2.8	55.8
5.0	279	246	276	238	282	249	286	241	281	251	280.8	4.6	245.0	7.7	56.2
6.0	357	307	349	299	354	312	355	303	351	313	353.2	4.5	306.8	8.1	55.5
7.0	381	378	383	379	392	382	398	386	394	383	389.6	10.6	381.6	4.3	55.7
7.5	419	419	412	412	423	423	426	426	428	428	421.6	8.5	421.6	8.5	56.2

[1] see Figure 7.

Figure 8 presents the equations of the trend lines of the measured forces F_{com} [N] (see Tables 1–8) in an XY dot chart in Microsoft Excel. The reliability value R measures the reliability of the trend line—the closer R^2 is to 1, the better the trend line fits the data.

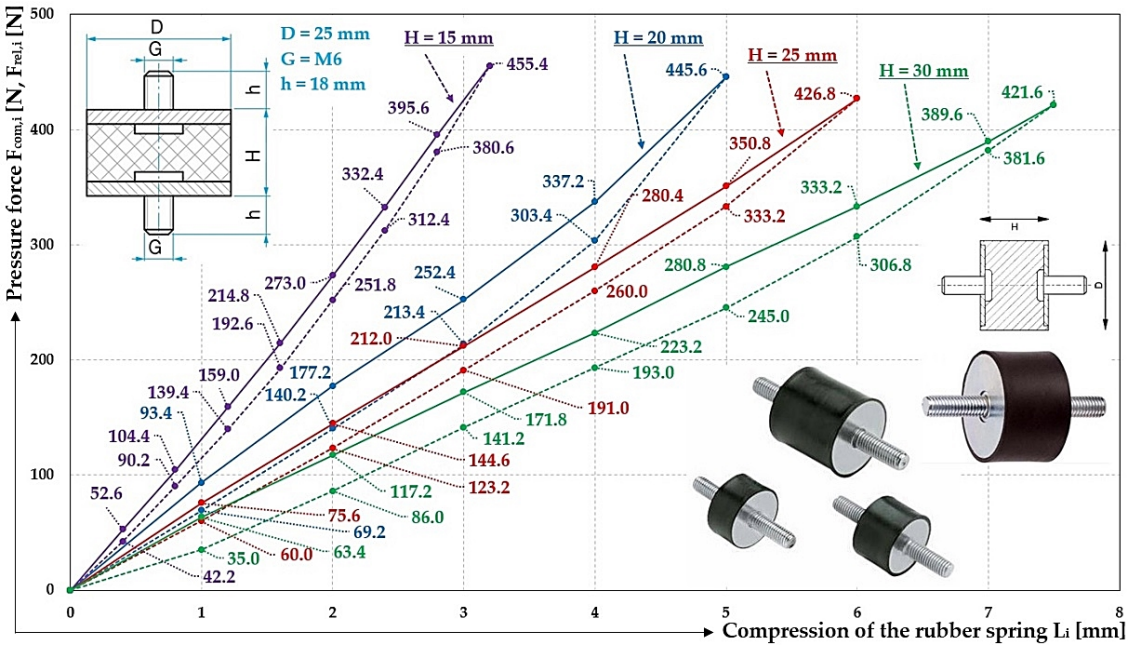

Figure 7. Graph of the dependence of the compressive force acting on a rubber spring ϕ25 mm with length in the unloaded state of H_0 = 15 ÷ 30 mm and its elastic deformation. H_0 (●) 15 mm, (●) 20 mm, (●) 25 mm, (●) 30 mm.

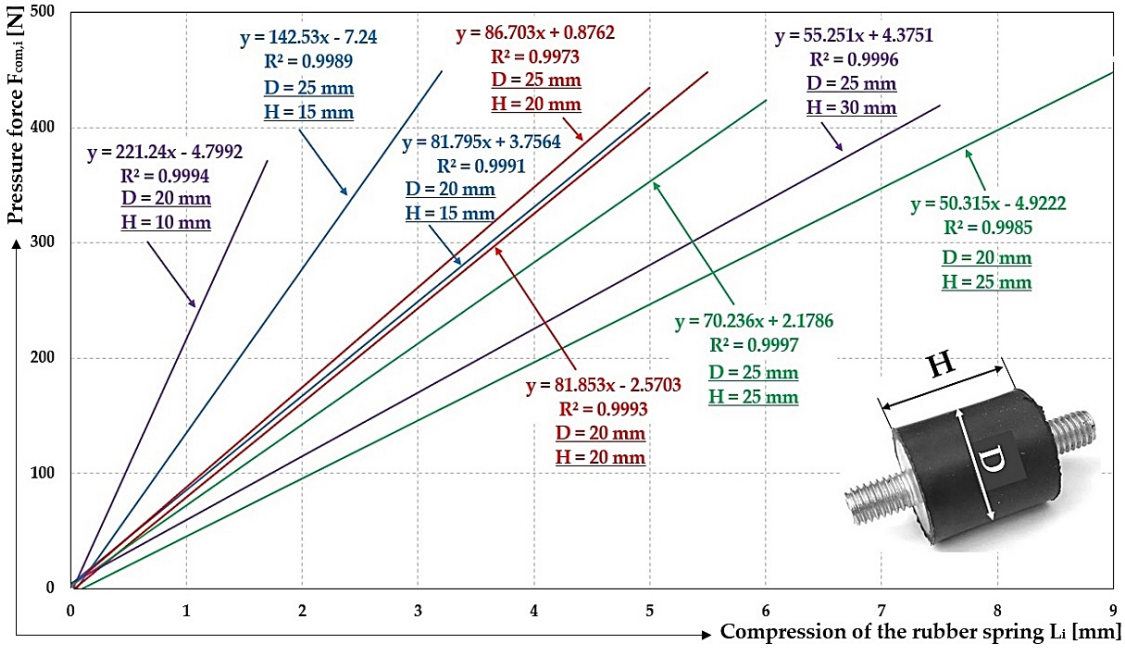

Figure 8. Equation of the trend lines of the measured forces acting on the silent blocks during elastic deformation.

3.2. Detection of Forces Acting on Force Blocks by Tension Pressure Sensor

The miniature sensor is designed for static and dynamic applications. Due to the high natural frequency of the transducer, it can also be used for dynamic force measurements. Characteristic mechanical quantities: natural frequence 5 KHz. Vibrational stress as per IEC 60068-2-27: 50 Hz. A sampling frequency of 500 Hz was used in the measurements.

The following tables (Tables 9–12) show the measured values of the compressive forces $F_{com,i}$ [N] of the silent blocks (ϕ20 mm and ϕ25 mm with unloaded length H_0 = 10 to 30 mm) during their compression, i.e., deformation L_i [m]. The tables show the values of F_{com} [N], which is the arithmetic mean of all (n = 3 number of replicate measurements) measured values of $F_{com,i}$ [N] and $\kappa_{\alpha,n}$ [-], which is the marginal error. $t_{\alpha,n}$ [-] $t_{5\%,3}$ = 4.30) is the Student's coefficient for the risk α [%] (α = 5%) and the confounding coefficient P [%] (P = 95%) [41].

Figure 9 presents measured values of the compressive force $F_{com,3}$ [N] at compression L_i [mm] of a rubber spring of diameter D = 20 mm, with length in the unloaded state of H_0 = 10 mm.

Table 9. Rubber spring D = 20 mm; length when not loaded H_0 = 10 mm and 15 mm.

i	1	2	3				i	1	2	3			
L_i	$F_{com,1}$	$F_{com,2}$	$F_{com,3}$ [3]	F_{com}	$\kappa_{5\%,3}$	$s_{s,com}$	L_i	$F_{com,1}$	$F_{com,2}$	$F_{com,3}$	F_{com}	$\kappa_{5\%,3}$	$s_{scom,i}$
mm			N			$N \cdot mm^{-1}$	mm			N			$N \cdot mm^{-1}$
0	0	0	0	0	0	-	0	0	0	0	0	0	-
0.2	52.3 [1]	51.5	47.5	50.4	4.6	280.2	0.2	16.2	16.8	18.3	17.1	1.9	85.5
0.6	181.6	180.3 [2]	176.8	179.6	4.3	299.3	1.3	108.1 [4]	108.5	108.8	108.5	0.6	83.4
0.9	278.3	277.8	273.5	276.5	4.7	307.3	2.0	164.1	162.9	162.6	163.2	1.4	81.6
1.3	417.9	421.4	413.1	417.5	6.8	321.1	2.8	229.4	226.6	225.8	227.3	3.3	81.2
1.7	592.8	602.0	588.0	594.3	12.0	349.6	3.6	305.1	297.3	298.4	300.3	7.5	83.4
							5.0	416.1	422.4	427.5	422.0	9.2	84.4

[1] see Figure 10a, [2] see Figure 10b, [3] see Figure 9, [4] see Figure 11a.

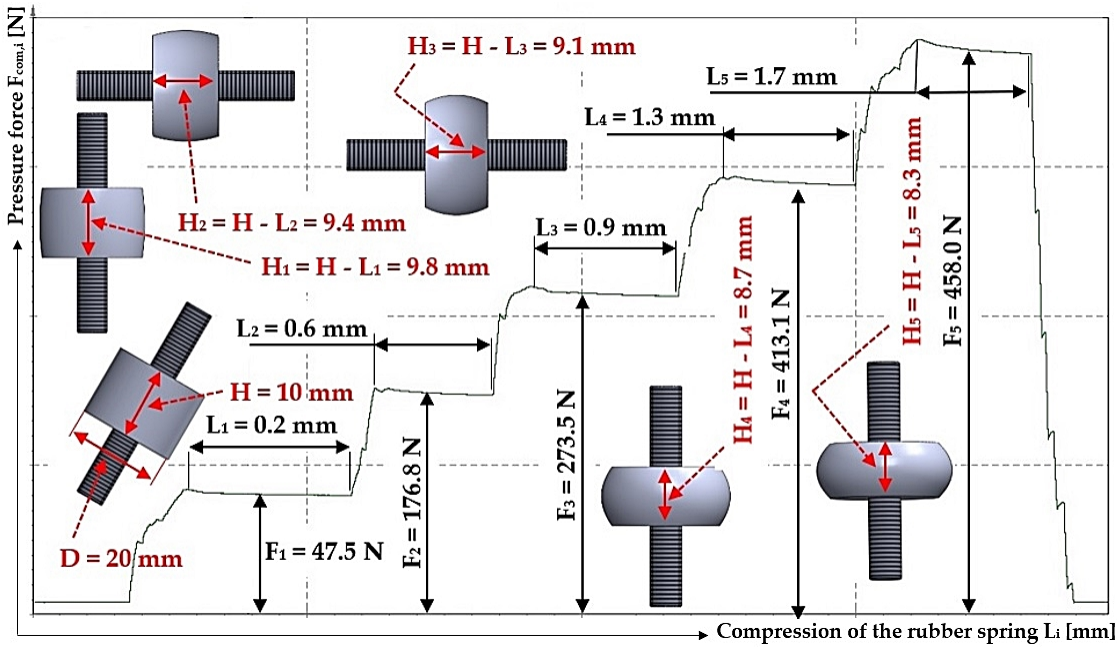

Figure 9. Measured values of the compressive force $F_{com,3}$ [N] at compression L_i [mm] of a rubber spring of diameter D = 20 mm, with length in the unloaded state of H_0 = 10 mm.

Figure 10 presents measured values of the compressive force $F_{com,3}$ [N] at compression L_i [mm] of a rubber spring of diameter D = 20 mm, with length in the unloaded state of H_0 = 10 mm.

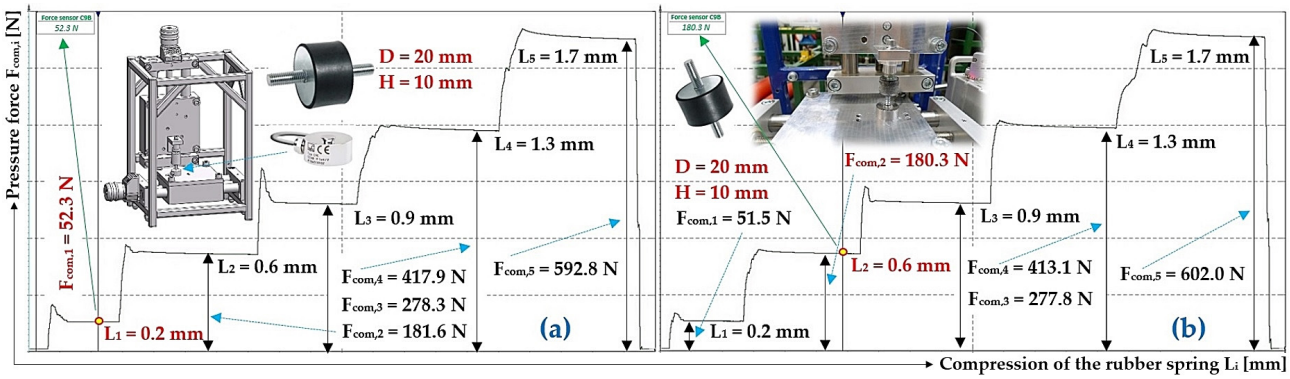

Figure 10. Measured values of the compressive force $F_{com,i}$ [N] during compression L_i [mm] of a rubber spring of diameter D = 20 mm, length H_0 = 10 mm. Compressive force $F_{com,1}$. (**a**) 52.3 N, (**b**) 108.1 N.

Figure 11 presents measured values of the compressive force $F_{com,3}$ [N] at compression L_i [mm] of a rubber spring of diameter D = 20 mm, with length in the unloaded state of H_0 = 10 mm.

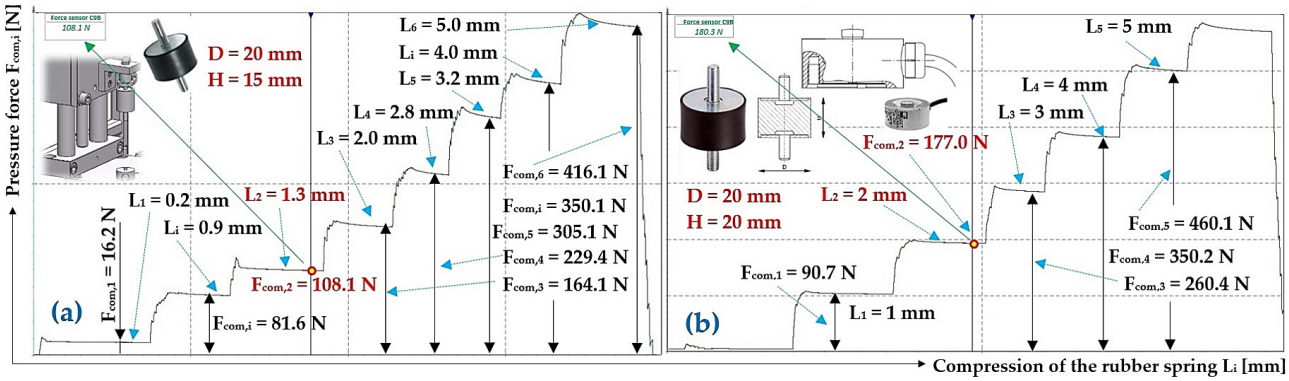

Figure 11. Measured values of the compressive force $F_{com,i}$ [N] during compression L_i [mm] of a rubber spring of diameter D = 20 mm, length H_0. (**a**) 15 mm, (**b**) 20 mm.

Table 10. Rubber spring D = 25 mm; length when not loaded H_0 = 20 mm and 25 mm.

i	1	2	3				i	1	2	3			
L_i	$F_{com,1}$	$F_{com,2}$	$F_{com,3}$	F_{com}	$\kappa_{5\%,3}$	$s_{Scom,i}$	L_i	$F_{com,1}$	$F_{com,2}$	$F_{com,3}$	F_{com}	$\kappa_{5\%,3}$	$s_{Scom,i}$
mm			N			N·mm^{-1}	mm			N			N·mm^{-1}
0	0	0	0	0	0	-	0	0	0	0	0	0	-
1	90.7	90.8	89.2	90.2	1.6	90.2	1	51.6	51.1	51.7	51.5	0.6	51.5
2	177.0 [1]	177.1	172.4	175.5	4.8	87.8	2	100.0	100.3	100.4	100.2	0.4	50.1
3	260.4	260.5	256.9	259.3	3.7	86.4	4	201.0 [2]	200.6	200.8	200.8	0.3	50.2
4	350.2	350.3	345.9	348.8	4.5	87.2	6	307.9	306.1	305.9	306.6	2.0	51.1
5	460.1	460.2	453.7	458.0	6.7	91.6	8	431.5	430.5	429.6	430.5	1.5	53.8
							9	506.9	510.6	511.5	509.7	4.3	56.6

[1] see Figure 11b, [2] see Figure 12a.

Figure 12 presents values of the compressive force $F_{com,i}$ [N] at compression L_i [mm] of a rubber spring of diameter D = 20 mm and 25 mm, with length in the unloaded state of H_0 = 15mm and 25 mm.

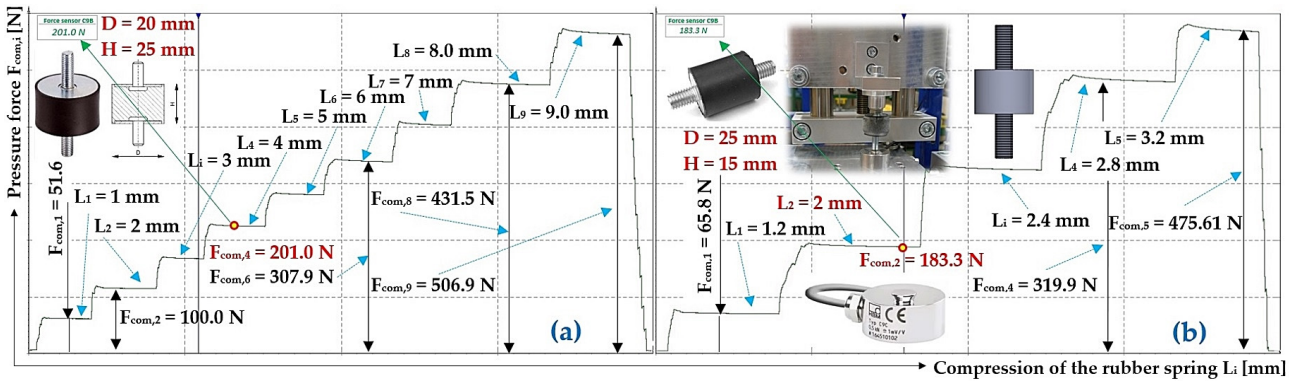

Figure 12. Measured values of the compressive force $F_{com,i}$ [N] during compression L_i [mm] of a rubber spring of diameter D = 20 mm and 25 mm, length H_0. (**a**) 25 mm, (**b**) 15 mm.

Table 11. Rubber spring D = 25 mm; length when not loaded H_0 = 15 mm and 20 mm.

i	1	2	3				i	1	2	3			
L_i	$F_{com,1}$	$F_{com,2}$	$F_{com,3}$	F_{com}	$\kappa_{5\%,3}$	$s_{scom,i}$	L_i	$F_{com,1}$	$F_{com,2}$	$F_{com,3}$	F_{com}	$\kappa_{5\%,3}$	$s_{scom,i}$
mm			N			$N \cdot mm^{-1}$	mm			N			$N \cdot mm^{-1}$
0	0	0	0	0	0	-	0	0	0	0	0	0	-
1.2	65.8	59.6	61.0	62.1	5.7	151.0	1	98.6	95.0	93.7	95.8	4.4	95.8
2	183.8 [1]	178.9	181.0	181.2	4.0	158.6	2	190.7	186.0	185.5	187.4	5.1	93.7
2.8	319.9	315.0	316.9	317.3	4.1	169.2	3	278.9 [2]	272.7	271.9	274.5	6.8	91.5
3.2	475.6	471.6	473.7	473.6	3.2	176.2	4	379.5	367.9	366.8	371.4	12.6	92.9
							5	492.9	496.8	494.7	494.8	3.1	99.0

[1] see Figure 12b, [2] see Figure 13a.

Figure 13 presents values of the compressive force $F_{com,i}$ [N] at compression L_i [mm] of a rubber spring of diameter D = 25 mm, with length in the unloaded state of H_0 = 25 mm and 30 mm.

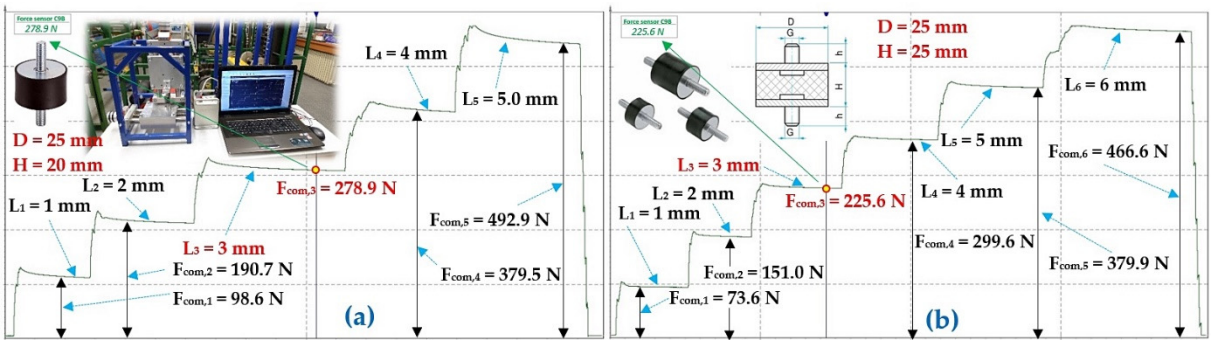

Figure 13. Measured values of the compressive force $F_{com,i}$ [N] during compression L_i [mm] of a rubber spring of diameter D = 25 mm, length H_0. (**a**) 20 mm, (**b**) 25 mm.

Table 12. Rubber spring D = 25 mm; length when not loaded H_0 = 25 mm and 30 mm.

i	1	2	3				i	1	2	3			
L_i	$F_{com,1}$	$F_{com,2}$	$F_{com,3}$	F_{com}	$\kappa_{5\%,3}$	$s_{scom,i}$	L_i	$F_{com,1}$	$F_{com,2}$	$F_{com,3}$	F_{com}	$\kappa_{5\%,3}$	$s_{scom,i}$
mm			N			$N \cdot mm^{-1}$	mm			N			$N \cdot mm^{-1}$
0	0	0	0	0	0	-	0	0	0	0	0	0	-
1	71.3	73.6	73.1	72.7	2.1	72.7	1	72.6	69.5	71.3	71.1	2.5	71.1
2	149.0	151.0	150.4	150.1	1.8	75.1	2	136.0	133.0	134.6	134.5	2.4	67.3
3	223.9	225.6 [1]	224.7	224.7	1.3	74.9	3	197.6	194.8	196.1	196.2	2.2	65.4
4	298.9	299.6	299.3	299.3	0.6	74.8	4	256.5	253.9	257.6	256.0	3.3	64.0
5	374.7	379.9	375.1	376.6	5.2	75.3	5	316.9	314.4	313.9	315.1	2.8	63.0
6	462.7	466.6	464.6	464.6	3.1	77.4	6	381.4	378.6	376.2	378.7	4.1	63.1
							7	448.8	447.7	447.0	447.8	1.5	64.0
							7.5	482.8	486.4	482.9	484.0	3.7	64.5

[1] see Figure 13b.

Figures 10 and 11 present the values of the measured compressive forces, randomly selected from Table 9. In case of interest, it is possible, upon written request by e-mail to the authors of this paper, to receive all measured data in data files with DXD extension (DEWESoft software) or XLS, XLSX (Microsoft Excel software). The same applies to the following presented tables.

Figure 14 shows the comparison of measured compressive forces $F_{com,i}$ [N] by digital force gauge DST-220A and tension pressure sensor C9B during the compression of rubber springs of diameter D = 20 mm with lengths in the unloaded state of H_0 = 10 ÷ 25 mm. The numerical values of the compressive forces F_{com} [N]—see Tables 1–4—given for the solid curves, correspond to measurement variant 1 (see Section 3.1); the values of the compressive forces F_{com} [N]—see Tables 9 and 10—given for the broken curves, correspond to measurement variation 2 (see Section 3.2).

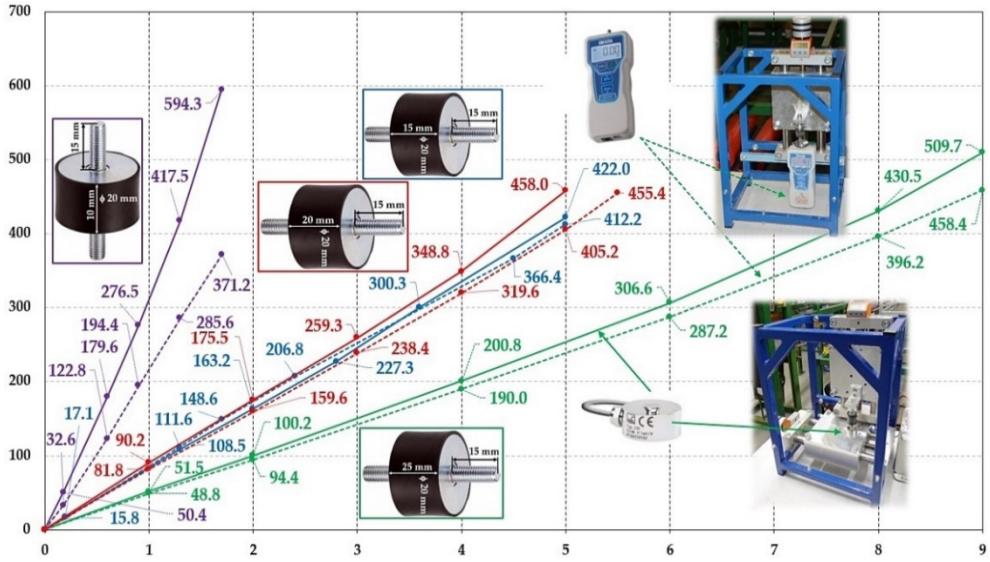

Figure 14. Measured values of compressive forces $F_{com,i}$ [N] of rubber spring D = 20 mm by digital force gauge DST-220A (solid curves) and tension pressure sensor C9B (dashed curves). Spring length in the unloaded state of H_0 [mm] (●) 10, (●) 15, (●) 20, (●) 25.

Figure 15 shows the comparison of measured compressive forces $F_{com,i}$ [N] with the digital force gauge DST-220A and the tension pressure sensor C9B during compression of rubber springs of diameter D = 25 mm with lengths in the unloaded state of $H_0 = 15 \div 30$ mm. The numerical values of the pressure forces $F_{com,i}$ [N]—see Tables 5–8—given for the solid curves, correspond to measurement variation 1 (see Section 3.1); the values of the pressure forces $F_{com,i}$ [N]—see Tables 11 and 12—given for the dashed curves, correspond to measurement variation 2 (see Section 3.2).

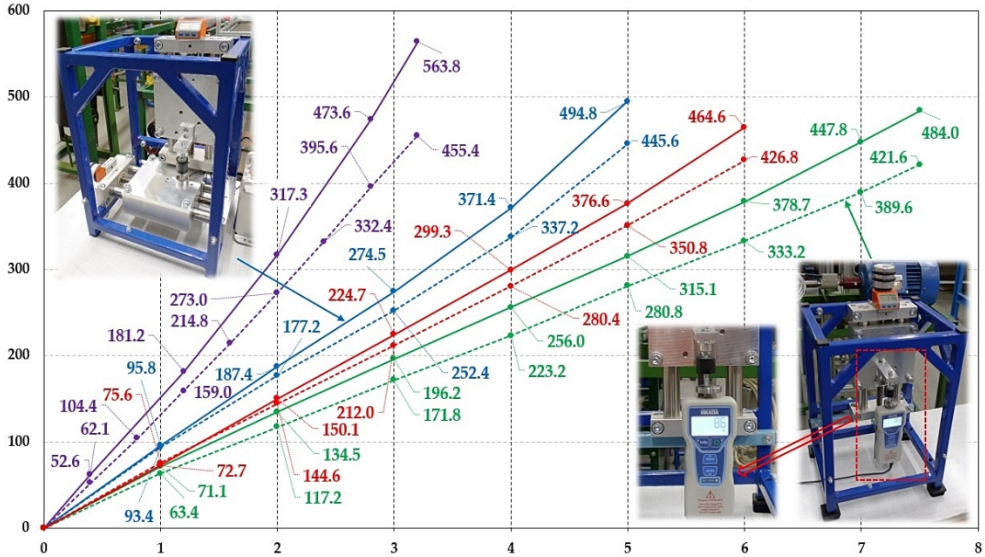

Figure 15. Measured values of compressive forces $F_{com,i}$ [N] of rubber spring D = 25 mm by digital force gauge DST-220A (solid curves) and tension pressure sensor C9B (dashed curves). Spring length in the unloaded state of H_0 [mm] (●) 15, (●) 20, (●) 25, (●) 30.

4. Discussion

Rubber springs made of elastic material (rubber) are used for various mechanical applications because of their ability to be deformed and then return to their original shape.

They can effectively absorb and dampen shocks or vibrations, making them suitable for use in automotive, machinery or conveying equipment where vibration needs to be eliminated.

The measurements of the compressive forces acting on the rubber springs presented in Figures 6 and 7 confirmed that the rubber springs have a progressive characteristic [42]. Progressive rubber springs [43,44] change their resistance to compression slowly at first and then more steeply, i.e., parabolically, with increasing load.

In Tables 1–8, the stiffnesses of the rubber springs $s_{scom,i}$ [N·mm^{-1}] ϕ20 mm and ϕ25 mm are calculated from the measured values of the compressive forces with the digital force gauge DST-220A acting on the rubber spring $F_{com,i}$ [N] and its elastic deformation L_i [m] during compression.

From the measured values, the calculated arithmetic average of the spring stiffness ϕ20 mm and the unloaded length H_0 = 15 mm—see Table 2—takes the value s_{scom} = 83.7 N·mm^{-1}. In Ref. [34], it is stated that s_s = 94 N·mm^{-1}, which implies that s_{scom} [N·mm^{-1}] is 89.0% of s_s [N·mm^{-1}].

The arithmetic diameter of the spring stiffness ϕ20 mm and the length in the unloaded state of H_0 = 20 mm, see Table 3, takes the value s_{scom} = 80.8 N·mm^{-1}. In Ref. [34], it is given as s_s = 52 N·mm^{-1}, which implies that s_{scom} [N·mm^{-1}] is 155.4% of s_s [N·mm^{-1}].

The arithmetic diameter of the spring stiffness ϕ20 mm and the length in the unloaded state of H_0 = 25 mm, see Table 4, takes the value s_{scom} = 48.6 N·mm^{-1}. In Ref. [34], it is given as s_s = 50 N·mm^{-1}, which implies that s_{scom} [N·mm^{-1}] is 97.2% of s_s [N·mm^{-1}].

The arithmetic diameter of the spring stiffness ϕ25 mm and the length in the unloaded state of H_0 = 15 mm, see Table 5, takes the value s_{scom} = 135.9 N·mm^{-1}. In Ref. [34], it is given as s_s = 183 N·mm^{-1}, which implies that s_{scom} [N·mm^{-1}] is 74.3% of s_s [N·mm^{-1}].

The arithmetic diameter of the spring stiffness ϕ25 mm and the length in the unloaded state of H_0 = 20 mm, see Table 6, takes the value s_{scom} = 87.9 N·mm^{-1}. In Ref. [34], it is given as s_s = 120 N·mm^{-1}, which implies that s_{scom} [N·mm^{-1}] is 73.3% of s_s [N·mm^{-1}].

The arithmetic diameter of the spring stiffness ϕ25 mm and the length in the unloaded state of H_0 = 25 mm, see Table 7, takes the value s_{scom} = 71.7 N·mm^{-1}. In Ref. [34], it is given as s_s = 108 N·mm^{-1}, which implies that s_{scom} [N·mm^{-1}] is 66.4% of s_s [N·mm^{-1}].

The arithmetic diameter of the spring stiffness ϕ25 mm and the length in the unloaded state of H_0 = 30 mm, see Table 8, takes the value s_{scom} = 57.3 N·mm^{-1}. In Ref. [34], it is given as s_s = 75 N·mm^{-1}, which implies that s_{scom} [N·mm^{-1}] is 76.4% of s_s [N·mm^{-1}].

When measuring the stiffness of the actual stiffness values of rubber springs on laboratory equipment—variation 1—the largest/smallest stiffness deviation was obtained for a rubber spring with a diameter 25/20 mm and an unloaded length of H_0 = 25 mm. Experiments have shown that the actual stiffnesses of rubber springs are lower compared to the values stated by the manufacturer, in the least favourable case, by 33.6%.

In Tables 9–12, the stiffnesses of the rubber spring $s_{scom,i}$ [N·mm^{-1}] ϕ20 mm and ϕ25 mm are calculated from the measured values of the compressive forces of the tension pressure sensor C9B acting on the rubber spring $F_{com,i}$ [N] and its elastic deformation L_i [m] during compression.

The arithmetic average of the spring stiffness ϕ20 mm and the unloaded length H_0 = 15 mm calculated from the measured values, see Table 9, takes the value s_{scom} = 83.3 N·mm^{-1}, and in Ref. [34], it is given as s_s = 94 N·mm^{-1}, which implies that s_{scom} [N·mm^{-1}] is 88.6% of s_s [N·mm^{-1}].

The arithmetic diameter of the spring stiffness ϕ20 mm and the length in the unloaded state of H_0 = 20 mm, see Table 10, takes the value s_{scom} = 88.6 N·mm^{-1}. In Ref. [34], it is given as s_s = 52 N·mm^{-1}, which implies that s_{scom} [N·mm^{-1}] is 121.0% of s_s [N·mm^{-1}].

The arithmetic diameter of the spring stiffness ϕ20 mm and the length in the unloaded state of H_0 = 25 mm, see Table 10, takes the value s_{scom} = 52.2 N·mm^{-1}. In Ref. [34], it is given as s_s = 50 N·mm^{-1}, which implies that s_{scom} [N·mm^{-1}] is 104.4% of s_s [N·mm^{-1}].

The arithmetic diameter of the spring stiffness ϕ25 mm and the length in the unloaded state of H_0 = 15 mm, see Table 11, takes the value s_{scom} = 162.1 N·mm^{-1}. In Ref. [34], it is given as s_s = 183 N·mm^{-1}, which implies that s_{scom} [N·mm^{-1}] is 88.6% of s_s [N·mm^{-1}].

The arithmetic diameter of the spring stiffness ϕ25 mm and the length in the unloaded state of H_0 = 20 mm, see Table 11, takes the value s_{scom} = 94.6 N·mm^{-1}. In Ref. [34], it is given as s_s = 120 N·mm^{-1}, which implies that s_{scom} [N·mm^{-1}] is 78.8% of s_s [N·mm^{-1}].

The arithmetic diameter of the spring stiffness ϕ25 mm and the length in the unloaded state of H_0 = 25 mm, see Table 12, takes the value s_{scom} = 75 N·mm^{-1}. In Ref. [34], it is given as s_s = 108 N·mm^{-1}, which implies that s_{scom} [N·mm^{-1}] is 96.4% of s_s [N·mm^{-1}].

The arithmetic diameter of the spring stiffness ϕ25 mm and the length in the unloaded state of H_0 = 30 mm, see Table 11, takes the value s_{scom} = 65.3 N·mm^{-1}. In Ref. [34], it is given as s_s = 75 N·mm^{-1}, which implies that s_{scom} [N·mm^{-1}] is 87.1% of s_s [N·mm^{-1}].

When measuring the stiffness of the actual stiffness values of rubber springs on laboratory equipment—variation 2—the largest/smallest stiffness deviation was obtained for a rubber spring with a diameter 25/20 mm and an unloaded length of H_0 = 25 mm.

The difference in the measured stiffness values of rubber springs compared to the values specified by the manufacturer may be caused by repeated loading of the springs or "aging" of the rubber, as a result of which the rubber springs present a lower stiffness value.

The measured values given in Tables 1–12 show that the stiffnesses of rubber springs $s_{scom,i}$ [N·mm^{-1}] are lower (except for the rubber spring ϕ20 mm in length in the unloaded state of H_0 = 20 mm, see Tables 3 and 10, and for H_0 = 25 mm, see Table 11) than the stiffness values of rubber springs of identical dimensions given in Ref. [34].

It is known that in the case of a linear spring, the resistance of the spring to compression increases linearly with increasing load. Progressive springs, which include rubber springs, first change their resistance to compression slowly with increasing load and then more steeply, i.e., parabolically. It follows that the stiffness of a progressive spring is not a constant, but changes (increases) depending on its compression.

It is therefore not possible to define the stiffness of a rubber spring as a constant, as is stated, for example, in Ref. [45]. From the measured values of the compressive forces (linear data set) $F_{com,i}$ [N] during compression of the rubber springs, linear trend lines were plotted in Microsoft Excel; see Figure 8. The trend line is the function that best describes the data; it is a linear function, the graphical presentation of which is a straight line. The trend line function is found by the least squares method. It can be seen from Figure 8 that the smaller diameter rubber springs (D = 20 mm) exhibit lower stiffness relative to the larger diameter rubber springs (D = 25 mm). It is also true that shorter length rubber springs have a higher stiffness than longer length rubber springs of the same diameter. Rubber springs of shorter lengths can be subjected to less maximum compression and more maximum load than rubber springs of a longer length of the same diameter.

Sensors applied to an actual working vibration machine are able to control its working activity or to control certain technical parameters to a certain extent. In the case of vibration machines, sensors can, for example, detect the load applied to the springs that support the trough/sorting screens. The correct operation of a particular vibration machine can be monitored automatically from the detection of spring stiffnesses determined precisely in advance in the laboratory (e.g., according to the procedure described in Section 3 of this paper). In vibrating machines, the instantaneous values of the compressive forces acting on the springs can be measured during their working operations and the amount of

conveyed/sorted material on the trough/sorting surface can be tracked according to the applied load.

Knowledge of experimentally obtained values of elastic deformations of rubber springs induced by applied compressive forces of known magnitudes is essential for the selection of rubber springs with optimal properties, which are used to dampen vibrations transmitted to the supporting parts of vibrating machines. By sensory monitoring of the pressure forces acting on the springs supporting the trough of vibratory conveyors—see Figure 16—it is possible to analyse, diagnose and automate the working operation of vibration machines in practice.

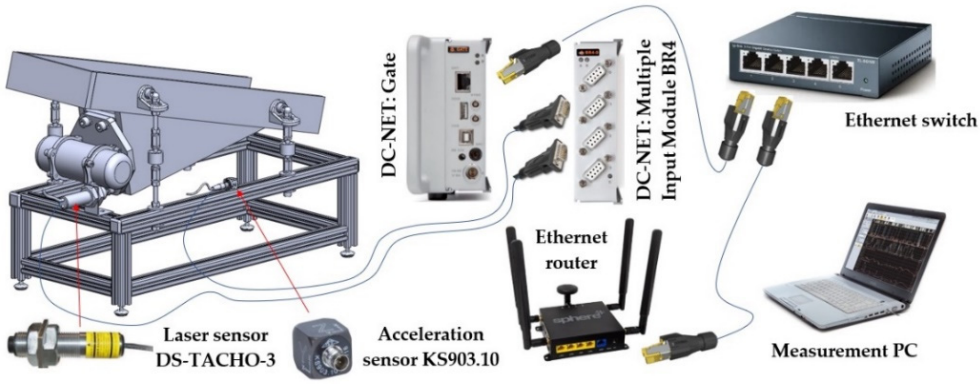

Figure 16. Rubber springs used to dampen the vibrations of the vibrating machine.

When using a strain tensometric force sensor, the magnitude of the measured pressure forces was evaluated by the DeweSoft DS-NET system, which was connected to an ethernet LAN, so the measured data could be processed, analysed and stored by any computer on the network.

5. Conclusions

The need for research can be characterized by the fact that in many vibrating machines it is necessary to eliminate the magnitude of vibrations transmitted to the machine frames. The optimal choice of spring (spring stiffness) in vibrating machines has a fundamental influence on the magnitude of vibrations transmitted to the floor (subsoil) of the building. The spring stiffness can be obtained by measuring on the laboratory equipment described in this article. The methodology for determining the stiffness of rubber springs on the laboratory equipment serves as input data for the machine being prepared—a vibrating conveyor. On this conveyor, vibrations of the conveyor frame will be measured by a vibration sensor based on the measured (precise values) of the stiffness of the rubber springs. The measured vibration signals will be sent to a PC via a Wi-Fi router for their analysis and verification that the conveyor is operating in the optimal mode.

Measuring the characteristics of rubber springs is an important process that involves testing not only stiffness and elasticity, but also behaviour under long-term or cyclic loading, which is essential to ensure the reliability and serviceability of springs in various applications.

In this paper, the compressive forces acting on rubber springs during their compression were measured on laboratory equipment using sensors. The relationship between the force acting on the spring and its elastic deformation can be used as an input value for control, diagnosis and monitoring of vibrating machines. Vibrating machines in the form of vibrating conveyors or sorters, using an electromagnetic vibration exciter as the source of excitation force, transmit high frequency vibrations to the substrate. By supporting the trough of vibratory conveyors with rubber springs of suitable stiffness, these springs can capture the high frequency oscillatory motion and attenuate the noise due to the high self-attenuation capability of the rubber.

The measurements carried out in a laboratory at the Department of Machine and Industrial Design, Faculty of Mechanical Engineering, VSB-Technical University of Ostrava, confirmed the progressivity of the rubber springs. The progressivity of a spring can be defined by the fact that its stiffness increases with increasing compression of the spring; the characteristic of the spring is not a straight line but an exponential. It has been shown that at half the compression, a rubber spring has less stiffness than a steel coil spring.

This is an attempt to select the most optimal spring from the actual stiffnesses of the measured rubber springs and use it as a spring to support the trough of a laboratory vibrating conveyor, which uses a single-phase asynchronous vibration motor to excite the trough vibrations. On the vibrating conveyor used in the study, sensors detect and the DEWESoft DS-NET measuring instrument monitors the pressure force acting on a selected number (or all) of the rubber springs supporting the trough of the vibrating conveyor. The electrical signal obtained by the tension pressure sensor will be used as an input parameter (digital input) to administer the automated operation and control of the vibrating conveyor, which fits with the current trend of digitalization and related automation of production known as Industry 4.0.

Author Contributions: Conceptualization, L.H.; methodology, L.H.; software, M.K.; validation, L.K. and J.B.; formal analysis, L.H.; investigation, L.H. and J.Š.; resources, J.B.; data curation, J.Š.; writing—original draft preparation, L.H.; writing—review and editing, L.H.; visualization, L.H. and M.K.; supervision, L.K.; project administration, L.H.; funding acquisition, L.H. All authors have read and agreed to the published version of the manuscript.

Funding: This research was funded by Research and innovation of modern processes and technologies in industrial practice grant number SP2024/001 and SP2025/001, and was funded by MŠMT ČR (Ministry of education youth and sports).

Data Availability Statement: Measured data of force values $F_{com,i}$ [N], which are listed from Tables 9–12 and processed using DEWESoft® X2 SP5X software, and measured data of pressure forces $F_{com,i}$ [N], which are listed from Tables 1–12 and processed using DEWESoft X software, can be sent in case of interest, by prior written agreement, in *.XLSX (Microsoft Excel) format.

Conflicts of Interest: The authors declare no conflicts of interest. The funders had no role in the design of the study, in the collection, analyses, or interpretation of data, in the writing of the manuscript, or in the decision to publish the results.

References

1. Murray, M.M.; Howle, L.E. Spring stiffness influence on an oscillating propulsor. *J. Fluids Struct.* **2003**, *17*, 915–926. [CrossRef]
2. Navarro, H.A.; de Souza Braun, M.P. Determination of the normal spring stiffness coefficient in the linear spring–dashpot contact model of discrete element method. *Powder Technol.* **2013**, *246*, 707–722. [CrossRef]
3. Hrabovsky, L.; Mlcak, T.; Kotajny, G. Forces generated in the parking brake of the pallet locking system. *Adv. Sci. Technol. Res. J.* **2019**, *13*, 181–187. [CrossRef] [PubMed]
4. Hrabovsky, L.; Dluhos, D. Calibration of transducers and of a coil compression spring constant on the testing equipment simulating the process of a pallet positioning in a rack cell. *Open Eng.* **2019**, *9*, 631–640. [CrossRef]
5. Soliman, A.M.A.; Allah, S.A.; El-Beter, A.A.; Hamid, M.S. Effect of suspension spring stiffness on vehicle dynamics. *Int. J. Heavy Veh. Syst.* **2001**, *8*, 316–334. [CrossRef]
6. Rączka, W. Testing of a spring with controllable stiffness. *Mech./AGH Univ. Sci. Technol.* **2006**, *25*, 79–86.
7. Loukidis, D.; Tamiolakis, G.P. Spatial distribution of Winkler spring stiffness for rectangular mat foundation analysis. *Eng. Struct.* **2017**, *153*, 443–459. [CrossRef]
8. Mlcak, T.; Zacek, V. Applied Forces in the Handling Unit Fixation Mechanism. *Teh. Vjesn.* **2022**, *29*, 620–627. [CrossRef]
9. Hrabovsky, L.; Fedorko, G.; Mlynek, L.; Michalik, P. Electromagnetic locking devices of car handling units. *Sci. J. Silesian Univ. Technol. Ser. Transp.* **2020**, *107*, 73–83. [CrossRef]
10. Vibration Motors. Available online: https://www.bevi.com/products/electric-motors/vibration-motors (accessed on 22 March 2024).
11. Noga, S.; Skrzat, A.; Stachowicz, F. Dynamic analysis of vibrating screener system. In *Journal of Physics: Conference Series*; IOP Publishing: Bristol, UK, 2013; Volume 451, p. 012028.

12. Feliks, J.; Tomach, P. The impact of vibrating screen startup time on vibration amplitude and energy consumption in transient state. *Energies* **2023**, *16*, 7129. [CrossRef]
13. Howell, L.L.; Midha, A. Evaluation of equivalent spring stiffness for use in a pseudo-rigid-body model of large-deflection compliant mechanisms. In *Proceedings of the International Design Engineering Technical Conferences and Computers and Information in Engineering Conference, Minneapolis, MN, USA, 11–14 September 1994*; American Society of Mechanical Engineers: New York, NY, USA, 1994; Volume 12846, pp. 405–412.
14. Hrabovsky, L. Validation Device for the Stiffness of Cylindrical Coiled Pressure Springs. *Acta Mech. Slovaca* **2020**, *24*, 42–48. [CrossRef]
15. Hrabovsky, L.; Molnar, V.; Kotajny, G.; Kulka, J. Pallet fixing lock, determination of shear resistance and spring stiffness. *Adv. Sci. Technol. Res. J.* **2020**, *14*, 190–197. [CrossRef]
16. Lefanti, R.; Ando, M.; Sukumaran, J. Fatigue and damage analysis of elastomeric silent block in light aircrafts. *Mater. Des. (1980–2015)* **2013**, *52*, 384–392. [CrossRef]
17. Ziobro, J. Analysis of suspension element of car body on the example silentblock. *Adv. Sci. Technol. Res. J.* **2015**, *9*, 125–129. [CrossRef] [PubMed]
18. Ozturk, B.; Kara, F. Finite Element-Based Simulation of Cooling Rate on the Material Properties of an Automobile Silent Block. *Adv. Mater. Sci. Eng.* **2020**, *2020*, 1954947. [CrossRef]
19. Fedotov, A.I.; Tikhov-Tinnikov, D.A.; Baradiev, V.S. Simulation of process of functioning silent blocks of car suspension. In *Proceedings of the International Conference "Aviamechanical Engineering and Transport" (AVENT 2018), Irkutsk National Research Technical University Irkutsk, Russian Federation 21-26 May 2018*; Atlantis Press: Amsterdam, The Netherlands, 2018; pp. 135–140.
20. Hatekar, H.; Anthonysamy, B.; Saishanker, V.; Pavuluri, L.; Pahwa, G.S. *Silent Block Bush Design and Optimization for Pick-Up Truck Leaf Spring*; No. 2017-01-0455, SAE Technical Paper; SAE International: Warrendale, PA, USA, 2017. [CrossRef]
21. Boiko, A.V.; Halezov, V.P.; Yan'kov, O.S.; Markov, A.S. System for measuring normal and tangential reactions distributed along the length of the contact patch of the tire with elastic flat supporting surface, The car for Siberia and the far North: The Design, operation, Economics. In Proceedings of the 90th International Scientific and Technical Conference of the Association of Automotive Engineers in the Irkutsk National Research Technical University, Tomsk Polytechnic University, Irkutsk, Russia, 21–26 May 2015; pp. 102–110, 482.
22. Fedotov, A.I.; Lisenko, A.V.; Tihov-Tinnikov, D.A. Control of the technical condition of the suspension of vehicles in operating conditions by the method of circular movement, The car for Siberia and the far North: The Design, operation, Economics. In Proceedings of the 90th International Scientific and Technical Conference of the Association of Automotive Engineers in the Irkutsk National Research Technical University, Irkutsk, Russia, 21–26 May 2015; pp. 232–238, 482.
23. Baradiev, V.S.; Tihov-Tinnikov, D.A. Experimental study of power characteristics of automotive silent blocks, Safety of wheeled vehicles in operation. In Proceedings of the 99th International Scientific and Technical Conference of the Association of Automotive Engineers in the Irkutsk National Research Technical University, Irkutsk National Research Technical University, Irkutsk, Russia, 15–18 March 2017; pp. 12–20, 570.
24. Misol, M.; Algermissen, S.; Monner, H.P. Experimental study of an active window for silent and comfortable vehicle cabins. In *Adaptive, Tolerant and Efficient Composite Structures*; Springer: Berlin/Heidelberg, Germany, 2012; pp. 439–447.
25. Luo, R.K.; Wu, W.X. Fatigue failure analysis of anti-vibration rubber spring. *Eng. Fail. Anal.* **2006**, *13*, 110–116. [CrossRef]
26. Berg, M. A non-linear rubber spring model for rail vehicle dynamics analysis. *Veh. Syst. Dyn.* **1998**, *30*, 197–212. [CrossRef]
27. Luo, R.; Shi, H.; Guo, J.; Huang, L.; Wang, J. A nonlinear rubber spring model for the dynamics simulation of a high-speed train. *Veh. Syst. Dyn.* **2020**, *58*, 1367–1384. [CrossRef]
28. Wu, J.; Shangguan, W.B. Modeling and applications of dynamic characteristics for rubber isolators using viscoelastic fractional derivative model. *Eng. Mech.* **2008**, *25*, 161–166.
29. Shi, H.L.; Wu, P.B.; Luo, R.; Zeng, J. Estimation of the damping effects of suspension systems on railway vehicles using wedge tests. *Proc. Inst. Mech. Eng. Part F J. Rail Rapid Transit* **2014**, *230*, 392–406. [CrossRef]
30. Misaji, K.; Hirose, S.; Shibata, K. Vibration analysis of rubber vibration isolators of vehicle using the restoring force model of power function type. *JSME Int. J. Ser. C Dyn. Control Robot. Des. Manuf.* **1995**, *38*, 679–685.
31. Austin, J.; Schepelmann, A.; Geyer, H. Control and evaluation of series elastic actuators with nonlinear rubber springs. In *Proceedings of the 2015 IEEE/RSJ International Conference on Intelligent Robots and Systems (IROS), Hamburg, Germany, 28 September–3 October 2015*; IEEE: Piscataway, NJ, USA, 2015; pp. 6563–6568.
32. Hsieh, W.H.; Tsai, C.H. Design and Analysis of a Novel Vibrating Conveyor. *Adv. Sci. Lett.* **2012**, *9*, 62–67. [CrossRef]
33. Rade, D.A.; De Albuquerque, E.B.; Figueira, L.C.; Carvalho, J.C.M. Piezoelectric driving of vibration conveyors: An experimental assessment. *Sensors* **2013**, *13*, 9174–9182. [CrossRef] [PubMed]
34. Silent Block ELESA a GANTER. Available online: https://www.elesa-ganter.cz/static/catalogues/files/Silentbloky.pdf (accessed on 16 June 2023).

35. DST-220A Digital Force Gauge. Available online: https://imada.com/products/dst-220a-digital-force-gauge/ (accessed on 21 July 2023).
36. C9C—Miniature Pressure Sensor. Available online: https://www.hbm.cz/en/produkty/kategorie/c9c/ (accessed on 13 May 2023).
37. Positioning Systems Manually Operated. Available online: https://mnsystems.cz/images/mm/Katalog/02_pt-system_19-07-10_dt-eng_katalog-mme_1.pdf (accessed on 28 November 2024).
38. Data Acquisition Software Force Logger Series. Available online: https://www.forcegauge.net/pdf/fl_e.pdf (accessed on 18 February 2022).
39. DewesoftX Previous Releases. Available online: https://dewesoft.com/download/dewesoftx-previous-releases (accessed on 9 June 2023).
40. DEWESoft General Catalog. Available online: https://d36j349d8rqm96.cloudfront.net/3/6/Dewesoft-DS-NET-Manual-EN.pdf (accessed on 2 May 2021).
41. Madr, V.; Knejzlik, J.; Kopecny, I.; Novotny, I. *Fyzikální Měření (In English: Physical Measurement)*; SNTL: Prague, Czech Republic, 1991; p. 304. ISBN 80-03-00266-4.
42. Thaijaroen, W.; Harrison, A.J.L. Nonlinear dynamic modelling of rubber isolators using six parameters based on parabolic spring, springpot, and smooth-slip friction element. *Polym. Test.* **2010**, *29*, 857–865. [CrossRef]
43. Moulton, A.E.; Turner, P.W. Rubber springs for vehicle suspension. *Proc. Inst. Mech. Eng. Automob. Div.* **1956**, *10*, 17–41. [CrossRef]
44. Sun, B.; Xu, Z.; Zhang, X. Parametric optimization of rubber spring of construction vehicle suspension. In *Global Design to Gain a Competitive Edge: An Holistic and Collaborative Design Approach based on Computational Tools*; Springer: London, UK, 2008; pp. 571–580.
45. Cylindrical Silent Blocks Type A (Screw/Screw). Available online: https://www.rubber.cz/silentbloky-valcove-typ-a (accessed on 2 May 2021).